Drug Design, Development and Therapy

Dovepress
Taylor & Francis Group

Open Access Full Text Article

ORIGINAL RESEARCH

Ginkgolide B Alleviates LPS-Induced Inhibition of Osteogenic Differentiation in Human Periodontal Ligament Stem Cells by Suppressing the p-IκBα/NF-κB Pathway

Simeng Du[1], Daiwei Yang[1], Qing Liu[2], Peng Yang[1], Zhaoyan Wu[1], Yvxing Zhang[1], Siyu Chen[1], Jun Zhang[1]

[1]Department of Orthodontics, School and Hospital of Stomatology, Cheeloo College of Medicine, Shandong University & Shandong Key Laboratory of Oral Tissue Regeneration & Shandong Engineering Research Center of Dental Materials and Oral Tissue Regeneration & Shandong Provincial Clinical Research Center for Oral Diseases, Jinan, Shandong, People's Republic of China; [2]Department of Orthodontics, Taian Maternal and Child Health Hospital, Taian, Shandong, People's Republic of China

Correspondence: Jun Zhang, Department of Orthodontics, School and Hospital of Stomatology, Cheeloo College of Medicine, Shandong University & Shandong Key Laboratory of Oral Tissue Regeneration & Shandong Engineering Research Center of Dental Materials and Oral Tissue Regeneration & Shandong Provincial Clinical Research Center for Oral Diseases, No. 44-1 Wenhua Road West, Jinan, Shandong, 250012, People's Republic of China, Tel +86 13953109816, Fax +86 53188382923, Email zhangj@sdu.edu.cn

Background: Ginkgolide B (GB) is a widely utilized natural anti-inflammatory drug in clinical practice. This study investigates GB's effects on human periodontal stem cells (HPDLSCs) osteogenic differentiation under inflammation and its underlying mechanism, while evaluating its protective role against periodontal destruction in a rat periodontitis model.

Methods: HPDLSCs were isolated and identified in vitro. Lipopolysaccharide (LPS) was used to establish an inflammatory environment. Proliferation and osteogenic differentiation of HPDLSCs were assessed using the Cell-counting Kit-8 (CCK-8), Alizarin Red Staining (ARS), quantitative calcium assay, alkaline phosphatase (ALP) staining and activity assay, and immunofluorescence assay. In addition, the expression of osteogenesis-related genes and proteins was detected by qRT-PCR and Western blot analysis. To verify the role of the NF-κB (nuclear factor kappa-B) pathway in this mechanism, the expression level of NF-κB pathway-related protein was detected by Western blot analysis after using BAY-11-7082 (a NF-κB signaling pathway inhibitor). The rat periodontitis model was established in vivo experiments. Micro-computed tomography (micro-CT) quantified alveolar bone loss, while immunohistochemical staining (IHC) assessed tissue remodeling. Tests were analyzed using GraphPad Prism 8 software. Differences between more than two groups were analyzed by one-way or two-way analysis of variance (ANOVA) followed by Tukey's test. Values of $p < 0.05$ were considered statistically significant.

Results: LPS treatment triggered inflammation and suppressed osteogenesis in HPDLSCs in vitro, while GB (25, 100 μM) reversed these effects. The results of the Western blot assay showed that both GB and BAY11-7082 exhibited similar inhibitory effects on the NF-κB pathway. In vivo, GB mitigated alveolar bone loss and inflammatory tissue destruction in periodontitis rats.

Conclusion: GB can mitigate periodontitis by blocking the NF-κB pathway, offering dual anti-inflammatory and bone-protective effects.

Keywords: periodontitis, natural products, osteogenic differentiation, BAY11-7082

Introduction

Periodontitis is a prevalent oral disease characterized by alveolar bone resorption and tooth loosening, posing a significant global health burden. Epidemiological data indicate that over 1 billion cases of severe periodontitis were reported globally in 2021, with projections suggesting a rise to 1.5 billion by 2050.[1] Left untreated, the disease can precipitate severe sequelae, including tooth loss, impaired mastication, and compromised nutrient absorption,[2–4] significantly diminishing patients' quality of life.[5] Beyond its local effects, periodontitis exacerbates systemic comorbidities

Received: 19 May 2025
Accepted: 2 September 2025
Published: 15 September 2025

and complicates dental interventions. For instance, periodontitis increases the risk of complications during orthodontic treatment,[6] necessitating the monitoring of biomarkers like periodontal microRNAs during treatment.[7] Periodontitis significantly increases the risk of peri-implantitis in patients receiving dental implants,[8] the treatment of which requires a combination of pharmacological therapy and mechanical debridement.[9] Systemically, periodontitis is linked to diabetes progression,[10] endothelial dysfunction,[11] and increases cardiovascular risk in metabolic syndrome patients.[12]

The current standard clinical protocol for periodontitis primarily relies on mechanical debridement (scaling and root planing) combined with antimicrobial therapy.[13] While this approach can effectively slow disease progression, its therapeutic efficacy is significantly constrained by the inherent physical barrier properties of dental plaque biofilms and the increasingly severe issue of antibiotic resistance. In this context, the development of novel antimicrobial agents derived from natural bioactive compounds, along with elucidation of their precise mechanisms of action, holds crucial clinical significance for overcoming current therapeutic limitations. The escalating global burden of inflammatory diseases has spurred interest in natural products as promising anti-inflammatory agents, owing to their multifaceted pharmacological profiles and favorable safety margins.[14] Ginkgolide B, a natural platelet-activating factor receptor antagonist, exhibits potent anti-inflammatory effects across diverse disease models.[15] The molecular structure of GB is shown in Figure 1A. It mitigates cardiac hypertrophy,[16] enhances muscle regeneration in aging,[17] and modulates inflammatory pathways, exhibiting broad therapeutic effects.

Periodontal stem cells have been widely used to investigate the regulatory activity of non-coding RNAs (including miRNAs such as miR-21-5p, miR-495-3p, and circRNAs), which serve as key epigenetic regulators of the NF-κB signaling pathway and its associated inflammatory networks in LPS-induced periodontitis and osteogenic differentiation processes.[18,19] The NF-κB signaling pathway serves as a master regulator of inflammatory responses, and its dysregulation contributes to the pathogenesis of numerous inflammatory diseases.[20] The NF-κB family comprises five subunits (c-Rel, p50, p52, p65/RelA, and RelB), which remain inactive in the cytoplasm through binding to inhibitory IκB proteins. LPS induces IκB-α phosphorylation and ubiquitination, culminating in its degradation. This releases NF-κB,

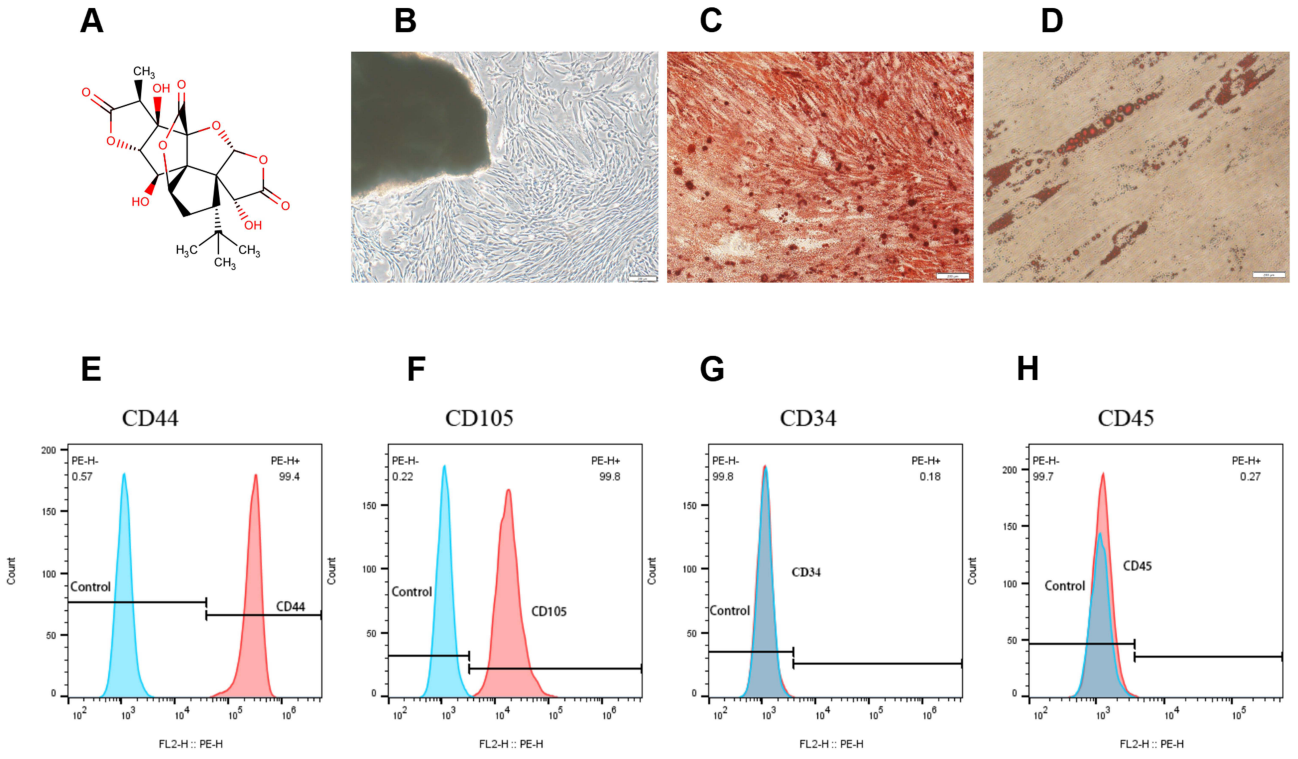

Figure 1 Culture and identification of HPDLSCs. (**A**) The molecular structure of ginkgolide B (GB; $C_{20}H_{24}O_{10}$). (**B**) Stellate-shaped cells migrated out from tissue blocks. Scale bar: 200 μm. (**C**) After osteogenic induction, HPDLSCs exhibited dark brown calcified nodules when stained with Alizarin Red. Scale bar: 200 μm. (**D**) After adipogenic induction, HPDLSCs exhibited lipid droplets of different sizes following Oil Red O staining. Scale bar: 200 μm. (**E**–**H**) Analysis of HPDLSCs surface marker expression by flow cytometry. CD44 (**E**) and CD105 (**F**) were highly expressed, while the expression of CD34 (**G**) and CD45 (**H**) was negative.

enabling its nuclear translocation, DNA binding, and transcriptional activation of pro-inflammatory genes.[21,22] The NF-κB pathway serves as a crucial therapeutic target for periodontitis. Research has demonstrated that BPIFA1 inhibits inflammation by regulating NF-κB/IκB signaling and macrophage polarization,[23] while sitagliptin alleviates inflammation and promotes osteogenesis through the AMPK/NF-κB pathway.[24] These findings provide novel targeted strategies for periodontitis treatment.

Notably, ginkgolide B has been demonstrated to mitigate myocardial injury via modulation of the A20-NF-κB pathway[25] and attenuate lung inflammation by suppressing TRIM37-mediated NF-κB activation.[26] Furthermore, ginkgolide B promotes osteogenic differentiation and ameliorates osteoporosis,[27,28] suggesting its broad therapeutic potential in inflammatory and bone-related disorders.

Our study is based on the following scientific rationale: (1) LPS-mediated NF-κB activation is an important pathogenic mechanism underlying periodontitis-associated osteogenic suppression; (2) GB has demonstrated NF-κB inhibitory effects in other inflammatory conditions; and (3) preliminary evidence suggests GB may promote osteogenic differentiation. Based on these findings, we hypothesize that GB may counteract LPS-induced suppression of osteogenic differentiation in human periodontal stem cells through NF-κB pathway modulation.

Materials and Methods

Isolation and Culture of HPDLSCs

This research was undertaken in compliance with the Declaration of Helsinki and received approval from the School of Stomatology Ethics Committee at Shandong University. (No. 20230907). The inclusion criteria for the selected samples were as follows: (1) Age range: Orthodontic patients aged 12–18 years requiring extraction of healthy premolars as part of orthodontic treatment. (2) Dental health status: No caries (no clinically or radiographically detectable decay); No periodontal disease; No periapical lesions; Informed consent obtained from both the patient and their legal guardian. (3) Sample collection timing: Extracted teeth were immediately placed in pre-cooled α-MEM medium (containing antibiotics) and processed within 4 hours. The exclusion criteria for the selected samples were as follows: (1) Systemic diseases: Presence of systemic conditions affecting periodontal or bone metabolism. (2) Medication influence: Recent use (within 3 months) of antibiotics, anti-inflammatory drugs, or medications affecting bone metabolism. (3) Local oral lesions: Teeth with developmental abnormalities, trauma history, restorations, or fillings. (4) Compliance issues: Refusal by the patient or guardian to participate. Immediately after extraction, teeth were stored in α-minimum essential medium (α-MEM; Yuanpei, Shanghai, China) supplemented with Penicillin-Streptomycin-Gentamicin Solution (100×; Biosharp, Guangzhou, China) at 4°C. Within 4 hours, samples were transferred to a sterile workstation, and root surfaces were rinsed with phosphate-buffered saline (PBS; Solarbio, Beijing, China). Periodontal tissue from the mid-root region was carefully dissected, fixed to culture flasks, and maintained upright with 5 mL of α-MEM containing 20% FBS (v/v) fetal bovine serum (FBS; Yeasen, Shanghai, China) and 1% (v/v) Penicillin-Streptomycin-Gentamicin Solution. After confirming tissue adherence, which needed approximately 4h, flasks were incubated horizontally at 37°C with 5% CO_2, with medium changes every 3 days. Spindle-shaped HPDLSCs migrated from tissue edges within 5–7 days. Upon reaching 70–80% confluence (typically after 14 days), cells were detached using 1.5 mL of trypsin solution (Biosharp, Guangzhou, China) and neutralized with complete medium (3 mL; 10% FBS). Isolated HPDLSCs were expanded via the limiting dilution method, and passages 3–5 (P3–P5) were used for subsequent experiments.

Flow Cytometry

HPDLSCs in the logarithmic growth phase were harvested, digested, centrifuged, and then resuspended in PBS and standardized the cell density to 1×10^7. Aliquots (100 μL) of cell suspension were distributed into five 1.5 mL EP tubes. Experimental groups were stained with the following fluorescently conjugated antibodies: CD34, CD44, CD45, and CD105 antibodies (Elabscience, Houston, TX, USA), while the control group received 100μL PBS alone. After 20 min of incubation at 4°C protected from light, cells were washed twice with PBS, resuspended in 500 μL PBS, and filtered through a nylon mesh. The flow cytometry was utilized for detection, and data analysis was conducted using FlowJo software (version 10, BD Biosciences, USA).

CCK-8 Assay

HPDLSCs were trypsinized, centrifuged, and resuspended in complete α-MEM medium. Cells were seeded in 96-well plates at a density of 3×10^3 cells/well (100 μL/well) and allowed to adhere for 24 h. Subsequently, cells were treated with LPS (1 μg/mL) and varying concentrations of GB (0, 25, 100, 400, and 1600 μM; purity ≥98%, Solarbio, Beijing, China) in quintuplicate.[29] At days 1, 3, and 5 post-treatment, 100 μL of 10% CCK-8 solution (Biosharp, Guangzhou, China) in α-MEM was added to each well. Following 45 min incubation at 37°C, absorbance was measured at 450 nm using a microplate reader (BMG Labtech, Ortenberg, Germany).

ARS and Calcium Quantification

For mineralization analysis, HPDLSCs were seeded in 6-well plates at a density of 1×10^5 cells/well and allowed to adhere for 24 hours. Upon reaching 80% confluence, the culture medium was replaced with osteogenic induction medium consisting of α-MEM supplemented with 10% FBS, 50 μg/mL ascorbic acid, 10 mM β-glycerophosphate, and 0.01 μM dexamethasone. The induction medium was refreshed every 3 days for 28 days. Following differentiation, cells were washed three times with PBS and fixed with 95% ethanol for 30 minutes at room temperature. After fixation, samples were stained with Alizarin Red S (Beyotime, Shanghai, China) for 20 minutes at 37°C, followed by five washes with distilled water to remove unbound dye. Mineralized nodules were documented using an inverted microscope (Olympus Corporation, Tokyo, Japan). For quantitative analysis, ARS-stained nodules were solubilized in 10% (w/v) cetylpyridinium chloride (CPC) eluent for 15 minutes with gentle agitation. The solubilized solution was centrifuged, and the supernatant absorbance was measured at 562 nm using a microplate reader.

Oil Red O Staining

HPDLSCs were cultured following the same seeding protocol as described for osteogenic induction. At 80% confluence, the medium was replaced with adipogenic induction medium consisting of α-MEM supplemented with 10% FBS, 0.5 M hydrocortisone, 500 mM isobutyl-methyl-xanthine, 60 mM indomethacin and 10 mM insulin. After 28 days of culture, cells were washed with PBS and fixed with 4% paraformaldehyde for 30 minutes at room temperature. After thorough PBS washing, the cells were stained with Oil Red O staining solution (Beyotime, Shanghai, China). Excess stain was removed by three washes with distilled water, and intracellular lipid droplets were visualized under an inverted microscope.

ALP Staining and ALP Activity Assay

HPDLSCs were inoculated in six-well plates at a density of 1×10^5 cells/well. Once the cells adhered, the medium was changed to osteogenic induction medium to continue the culture for 14 days. Subsequently, ALP staining was performed for analysis. After the cells were rinsed with PBS and fixed in 4% formaldehyde, they were stained using the BCIP/NBT Alkaline Phosphatase Colorimetric Assay kit (Beyotime, Shanghai, China). The level of ALP activity was observed qualitatively by the depth of the blue precipitation, with darker blue staining indicating a higher ALP activity, which indicated osteogenic differentiation.

After 14 days of osteogenic induction using the same cell culture method, the cells were rinsed with pre-cooled PBS, lysed on ice for 15 min by adding 100 μL of cell lysate (RIPA buffer: PMSF = 99:1, Beyotime, Shanghai, China), centrifuged, and the supernatant was extracted to measure the ALP activity using the Alkaline Phosphatase Assay Kit (Solarbio, Beijing, China). The protein concentration in the supernatant was also quantified using the BCA Protein Assay Kit (Solarbio, Beijing, China). Protein samples were mixed with 5× SDS-PAGE loading buffer (Beyotime, Shanghai, China) and heated at 100°C for 5 min to denature one side.

RNA Extraction and qRT-PCR Analysis

Following 14 days of osteogenic induction, total RNA was extracted using the Trizol method, and the extracted RNA was reverse transcribed into complementary DNA (cDNA) through a two-step process utilizing the Strand cDNA Synthesis Kit (Yeasen, Shanghai, China). The qRT-PCR reaction system was set up with 5 replicate wells, and the primer sequences were as follows:

- IL-6: 5′- ATAACCACCCCTG ACCCAAC-3′ and 5′-CCCATGCTACATTTGCCG AA-3′
- IL-8: 5′-TCAG AG ACAGCAG AGCACAC-3′ and 5′-GGCAAATGCACTTTCACACA-3′
- ALP: 5′-GGCGGTGAACGAGAGAATGT-3′ and 5′-GGACGTAGTTCTGCTCGTGG-3′
- RUNX-2: 5′-GGAGTGGACGAGGCAAGAGT-3′ and 5′-AGGCGGTCAGAGAACAAACT-3′
- COL-1: 5′-TAAAGGGTCACCGTGGCTTC-3′ and 5′-GGGAGACCGTTGAGTCCATC-3′
- GAPDH: 5′-GCACCGTCAAGGCTGAGAAC-3′ and 5′-TGGTGAAGACGCCAGTGGA-3′

Relative gene expression was calculated using the $2^{-\Delta\Delta Ct}$ method with GAPDH as the endogenous control, and all experiments were repeated five times.

Western Blot Analysis

Equal protein samples (20μg/lane) were taken, and the target proteins with different molecular weights were separated by electrophoresis using 8% SDS-PAGE. After transferring the target proteins onto the PVDF membrane, the membrane was blocked using rapid blocking solution (Servicebio, Wuhan, China) for 15 min at room temperature. After thorough washing with Tris-buffered saline containing 0.1% Tween 20 (TBST) (Beyotime, Shanghai, China), the samples were incubated overnight at 4 °C with the following primary antibodies: anti-ALP (1:1000; Proteintech, Hubei, China), anti-RUNX2 (1:1000; ImmunoWay, Plano, TX, USA), anti-COL-1 (1:1000; Proteintech, Hubei, China) and anti-GAPDH (1:5000; Proteintech, Hubei, China) as loading control. After three 10-minute washes with TBST, the membranes were incubated with the secondary antibody corresponding to the primary antibody for 1 hour at room temperature. After another thorough washing with TBST solution, a chemiluminescent substrate (Yeasen, Shanghai, China) was used with the Chemiluminescence Imaging System (Amersham Imager 600; GE Healthcare, Little Chalfont, UK). Band intensities were quantified using Image J, and the data were normalized for statistical analysis. Each experiment was repeated five times.

Immunofluorescence Assay

The treated cells were fixed with 4% paraformaldehyde for 30 min at 20–25°C. After three washes with PBS, cells were permeabilized with 0.1% Triton X-100 (Solarbio, Beijing, China) for 12 minutes. Subsequently, non-specific binding sites were blocked with 5% bovine serum albumin (BSA-V; Solarbio, Beijing, China) for 1 hour, and then incubated with primary antibody against COL-1 (1:200; Proteintech, Hubei, China) at 4°C overnight. After thorough washing with PBS (3 × 5 minutes), samples were incubated with fluorescein (FITC)-conjugated affinity pure goat anti-rabbit IgG (H + L) (1:200, SA00013-2) for 1 hour at room temperature in the dark. Subsequently, the cell nuclei were stained with 4,6-diamidino-2-phenylindole (DAPI; Solarbio, Beijing, China). Observation and image capture were performed with a fluorescence microscope (Leica, Wetzlar, Germany), and image analysis and fluorescence intensity quantification were performed using ImageJ software (National Institutes of Health, Bethesda, MD, USA).

NF-κB Pathway Studies

To investigate the role of the NF-κB pathway in the osteogenic differentiation of HPDLSCs, one of the known inhibitors of the NF-κB pathway, BAY11-7082 (1 μM), was used as a positive control in the experiment. The specific methods were as follows: HPDLSCs were seeded in 6-well plates at a density of 1×10^5 cells/well. After 14 days of osteogenic induction culture, LPS was added at different time points to activate the NF-κB pathway. Protein within hPDLSC was then isolated and analyzed for phospho-NF-κB p65 (Ser536) expression to determine peak pathway activation.

Subsequently, cells pretreated for 48 hours with either BAY 11–7082 (1 μM) or GB (100 μM) were stimulated with LPS (1 μg/mL). Total cellular protein was extracted and subjected to Western blot analysis using specific antibodies against phospho-NF-κB (1:1000; Abways, Shanghai, China), NF-κB (1:5000; Abways, Shanghai, China), phospho-IKBα (1:1000; Abways, Shanghai, China) and IKBα (1:1000; Abways, Shanghai, China). The level of protein expression was quantified using ImageJ software. All experiments were performed with five biological replicates to ensure statistical reliability.

Establishment of the Periodontitis Model

24 male Wistar rats (8 weeks old, average weight 180±5 g, purchased from Beijing Viton Lever Laboratory Animal Technology Co., Ltd.) were housed under specific pathogen-free (SPF) conditions with controlled environmental

parameters (temperature: 22±2°C, relative humidity: 65±5%, 12-hour light-dark cycle, noise level <60 dB). The nutritional intake of rats was ensured through adequate food and clean water consumed ad libitum, and bedding was replaced every 3 days to maintain hygienic conditions. The required size of experimental animals was calculated according to the resource equation method. Detailed methods are described in Supplementary Data 1. All experiments involving rats followed the National Institutes of Health Guide for the Care and Use of Laboratory Animals and were approved by the Institutional Animal Care and Use Committee of Shandong University (NO.20230907).

After one week of acclimatization feeding for all animals, the rats were randomly divided into four experimental groups (n=6 per group): (1) control, (2) periodontitis model, (3) low-dose GB treatment (5 mg/kg/day), and (4) high-dose GB treatment (20 mg/kg/day). Periodontitis models were established in the latter three groups and induced under isoflurane anesthesia (Yipin Pharmaceutical Co., Ltd, Hebei, China) by placing sterile 4–0 silk ligatures around the maxillary second molars. The specific methods were as follows: The rats were anesthetized using the inhalation anesthetic isoflurane, fixed in the supine position, with the maxilla exposed, and the silk threads were clamped with curved tweezers to pass through the space between the second and third molars, after which the threads located in the buccal region were passed through the space between the first and second molars in the same way, and the wire was adjusted to secure the knot at the palatal cervical region, and then trimmed excess thread with ophthalmic scissors. After the periodontitis model was established, rats in the GB low and high-dose groups received daily intraperitoneal injections of GB (dissolved in sterile saline) at their respective doses for 14 consecutive days, while animals in the other two groups received equivalent volumes of saline.

Micro CT

Following transcardial perfusion with 4% paraformaldehyde under deep anesthesia, the maxilla was carefully dissected and post-fixed in 4% paraformaldehyde at 4°C for 24 hours. After thorough PBS washing and air-drying, specimens were mounted on a scanning platform using low-density foam for micro-CT analysis (Quantum GX 2, PerkinElmer, USA) at 90 kV, 88 μA, with a thickness of 36 μm per layer. The scanned area comprised the three maxillary molars and their adjacent alveolar bone. After each 15-minute scanning process, the Micro-CT imaging data were imported in DICOM format, which underwent comprehensive analysis using a multi-software approach. Three-dimensional reconstruction was performed in Avizo 9.0 (Thermo Fisher Scientific, USA), incorporating manual alignment corrections in all anatomical planes using DataViewer software to ensure proper spatial orientation. The morphometric assessment was conducted in RadiAnt DICOM Viewer (Medixant, Poznan, Poland), with six standardized measurement sites per first molar (three buccal and three lingual locations) to quantify the linear distance from cemento-enamel junction to alveolar bone crest (CEJ-ABC). For microarchitectural evaluation, the interdental alveolar bone region between the first and second molars was analyzed in CTAn (CT analysis software; Skyscan NV) to compute microstructure parameters of the region of interest (ROI), including bone mineral density (BMD) and bone volume/total volume (BV/TV).

HE, MASSON and TRAP Staining

Samples were decalcified in 10% EDTA solution (pH 7.2) for 12 weeks. After complete decalcification confirmed by radiography and physical testing, tissues underwent graded ethanol dehydration, xylene clearing, and paraffin embedding. Subsequently, the specimens were cut from proximal to distal, and the thickness of paraffin sections was 4 μm. HE staining and MASSON staining of slides were performed to observe morphological changes in periodontal tissues. Tartrate-resistant acid phosphatase (TRAP) staining was employed to identify osteoclasts using the TRAP staining kit (Solarbio, Beijing, China). For quantitative analysis, TRAP-positive multinucleated cells (≥3 nuclei) adjacent to bone surfaces were counted and analyzed by ImageJ software.

IHC Staining

Following high-temperature antigen retrieval in citrate buffer, tissue sections were blocked with 5% goat serum for 40 minutes to prevent nonspecific binding. Primary antibodies were applied overnight at 4°C in a humidified chamber, including polyclonal anti-rabbit RUNX2 (1:200; ImmunoWay, Plano, TX, USA) and RANKL (1:300; ImmunoWay, Plano, TX, USA). After thorough washing, sections were incubated with biotin-labeled goat anti-rabbit IgG secondary

antibody for a minimum of 30 minutes. Upon completion of the washing process, immunoreactivity was visualized using the SP reagent kit (Solarbio, Beijing, China). Following hematoxylin counterstaining, a microscopic examination of the section was performed. Average optical density (AOD) values were determined using ImageJ software.

Data Analysis

A double-blind method was used for data collection, and all assays were repeated five times. Normality and homogeneity of variance were assessed using Shapiro–Wilk and F-tests, respectively. One-way or two-way ANOVA was conducted using GraphPad Prism software (version 8, MacKiev Software, Boston, MA, USA) to compare the differences between the groups. Tukey's test was used for post hoc analysis. Data were expressed as mean ± standard deviation. $P < 0.05$ was considered statistically significant.

Results

Isolation, Culture and Identification of HPDLSCs

After 1 week of primary culture, homogeneous spindle and stellate cells were seen migrating out from the edge of the tissue mass (Figure 1B). Observation of calcified nodules and lipid droplets using the ARS assay (Figure 1C) and Oil Red O staining (Figure 1D), respectively, confirmed that HPDLSCs can differentiate in multiple directions. Flow cytometry analysis of surface markers established a mesenchymal stem cell phenotype, with high expression of CD44 and CD105 (Figure 1E and F), while hematopoietic markers CD34 (Figure 1G) and CD45 (Figure 1H) showed minimal expression, confirming that the obtained cells were purified MSCs.

Effect of GB and LPS on Proliferation and Osteogenic Differentiation of HPDLSCs

CCK-8 assay showed that 1 μg/mL LPS treatment for 1/3/5 days had no significant effect on the proliferation of HPDLSCs ($P > 0.05$ vs control). In contrast, GB treatment demonstrated concentration-dependent proliferative effects, with both 25 μM and 100 μM concentrations significantly enhancing cell proliferation compared to untreated controls ($P < 0.001$ vs control) (Figure 2A–D).

ALP activity assay showed that 1 μg/mL LPS significantly inhibited osteogenesis in HPDLSCs ($P < 0.001$ vs control). Low concentrations (25 μM, 100 μM) of GB showed a dose-dependent reversal of the inhibitory effect of LPS, while high concentrations (400 μM, 1600 μM) of GB had an inhibitory effect on osteogenesis ($P < 0.001$ vs.LPS alone) (Figure 2E). Therefore, subsequent experiments were performed under 1 μg/mL LPS and low concentration (25 μM, 100 μM) GB treatment.

GB Reverses the Inhibitory Effect of LPS on Osteogenic Differentiation of HPDLSCs

Our experimental results demonstrated that GB effectively counteracts LPS-mediated suppression of osteogenic differentiation in HPDLSCs through multiple complementary assays. ALP staining showed that the degree of staining in the LPS-treated group was lighter than that in the control group, while GB co-treatment (25, 100 μM) reversed that, with 100 μM GB achieving nearly complete recovery (Figure 2F). ALP activity assays provided further validation, showing LPS suppressed the activity, with complete restoration following 100 μM GB treatment ($P < 0.001$) (Figure 2G). Mineralization capacity showed parallel results, as evidenced by ARS where LPS reduced nodule formation, while GB co-treatment (25,100 μM) restored mineralization (Figure 2H). Quantitative calcium measurements confirmed these observations, showing the same trend as the alizarin red staining assay ($P < 0.001$) (Figure 2I). These consistent findings across multiple osteogenic parameters establish that GB effectively reverses LPS-induced inhibition of osteogenic differentiation in a concentration-dependent manner, with 100 μM GB demonstrating optimal efficacy.

GB Reversed the LPS-Induced Decrease in the Expression Levels of Osteogenic-Related Makers in HPDLSCs

Molecular analysis at both gene and protein levels demonstrated that GB could counteract LPS-mediated inhibition of osteogenic differentiation. qRT-PCR showed that the expression of the osteogenesis-promoting related genes ALP

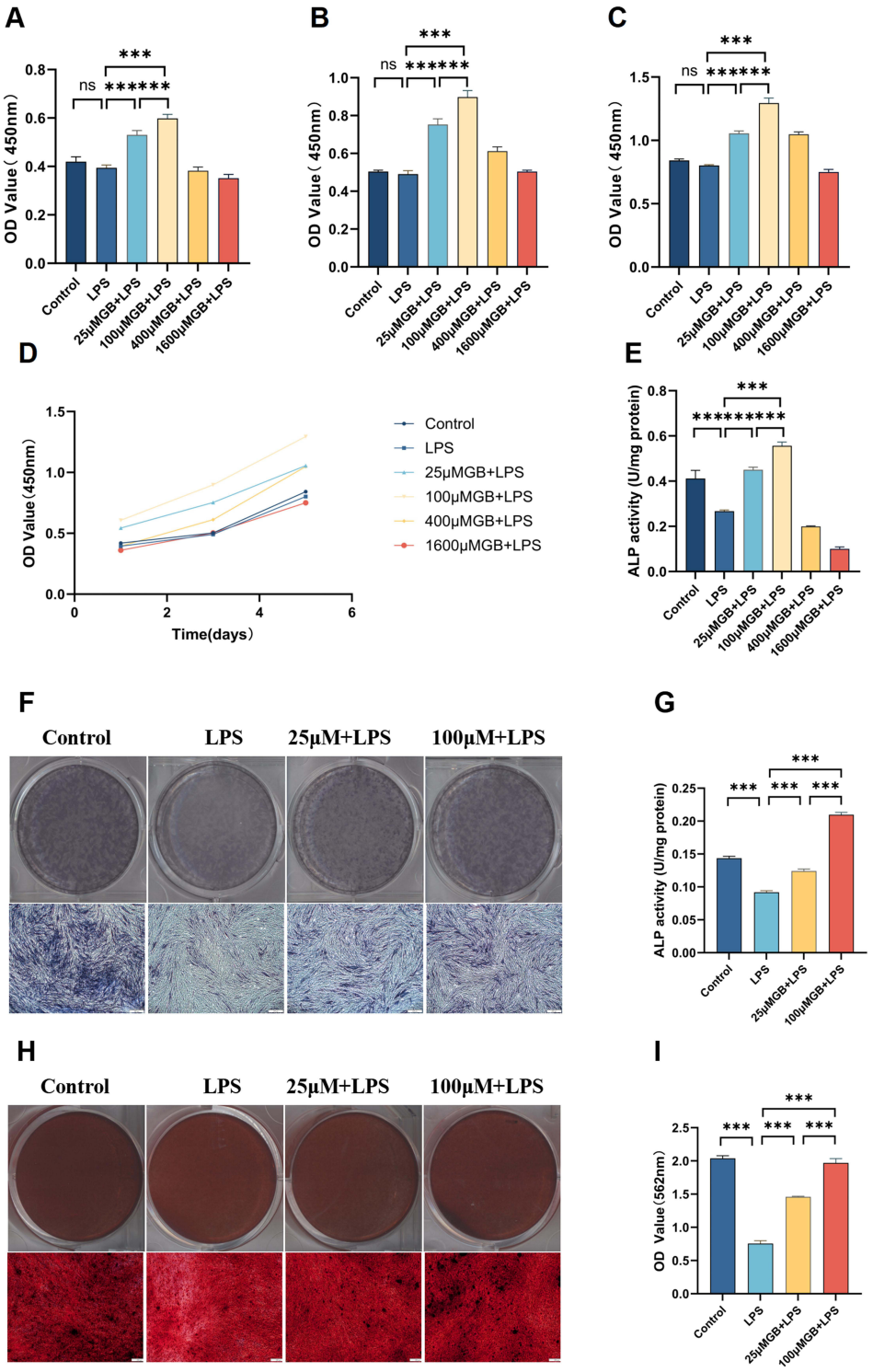

Figure 2 Effects of LPS and ginkgolide B on proliferation and osteogenic differentiation of HPDLSCs. (**A**–**C**) CCK-8 assay demonstrated the proliferation of HPDLSCs treated for 1 (A), 3 (B), 5 (**C**) days with control, LPS (1 μg/mL) or ginkgolide B (25 μM, 100 μM, 400 μM, 1600 μM). ("ns" indicates that the use of LPS shows no significant cytotoxic effects on HPDLSCs) (**D**) The growth curves of the control, LPS or ginkgolide B treated at different concentrations on day 1, 3, 5. (**E**) ALP activity under control, LPS (1 μg/mL) or LPS (1 μg/mL) and ginkgolide B (10 μM, 40 μM, 160 μM, 640 μM) treatment. (**F**) ALP staining under control, LPS (1 μg/mL) or LPS (1 μg/mL) and ginkgolide B (25 μM, 100 μM) treatment for 7 days. Scale bar: 200 μm. (**G**) ALP activity under control, LPS (1 μg/mL) or LPS (1 μg/mL) and ginkgolide B (25 μM, 100 μM) treatment for 7 days (one-way ANOVA). Error bars stand for mean ± SD. ***P < 0.001. (**H**) Formation of mineralized nodules under control, LPS (1 μg/mL) or LPS (1 μg/mL) and ginkgolide B (25 μM, 100 μM) treatment for 28 days. Scale bar: 200 μm. (**I**) Extracellular matrix mineralisation was assessed at OD562 (one-way ANOVA). Error bars stand for mean ± SD. ***P < 0.001. Each experiment was repeated five times.

 https://doi.org/10.2147/DDDT.S541290

(Figure 3A), RUNX-2 (Figure 3B), and COL-1 (Figure 3C) was down-regulated in HPDLSCs relative to control levels, while GB co-treatment produced a concentration-dependent restoration of gene expression ($P < 0.05$, $P < 0.01$, $P < 0.001$). The Western blot analysis showed parallel protein expression patterns (Figure 3D), with LPS treatment constituting a significant decrease in the expression levels of osteogenesis-related protein, while GB dose-dependently reversed the expression of osteogenesis-related protein caused by LPS. The protein expression level of ALP (Figure 3E), RUNX-2 (Figure 3F) and COL-1 (Figure 3G) was upregulated ($P < 0.001$). Immunofluorescence quantification further confirmed these findings, demonstrating that LPS reduced COL-1 intensity, while 100 μM GB treatment significantly restored fluorescence intensity ($P < 0.001$) (Figure 2H and I). These results of comprehensive molecular analysis established that GB effectively rescued the expression of key osteogenic markers at both transcriptional and translational levels in LPS-treated HPDLSCs.

GB Reduces LPS-Induced Inflammatory Cytokine Expression in HPDLSCs

Gene expression analysis revealed that LPS stimulation (1 μg/mL) triggered a robust inflammatory response in HPDLSCs, significantly upregulating IL-6 and IL-8 mRNA expression. Notably, GB co-treatment demonstrated potent anti-inflammatory effects, with both concentrations (25 μM and 100 μM) significantly reducing cytokine overexpression. The 100 μM GB treatment was particularly effective ($P < 0.001$). These findings demonstrate that GB not only promoted osteogenic differentiation but also effectively mitigated LPS-induced inflammatory signaling in HPDLSCs (Figure 3J and K).

GB Promotes Osteogenic Differentiation Through NF-κB Pathway Regulation in LPS-Induced Inflammatory Microenvironments

A double-blind method was used for data collection, and all assays were repeated five times.

To elucidate the molecular mechanism by which GB regulates the osteogenic differentiation of HPDLSCs, we tested the role of the NF-κB pathway in it. ALP staining, alizarin red staining, and quantitative calcium analysis showed that the GB and BAY11-7082-treated groups had deeper staining (Figure 4A and B) and increased calcium deposition content compared with the LPS-treated group alone ($P < 0.001$) (Figure 4C). The experimental results showed that both 100 μM GB and BAY11-7082 (NF-κB pathway inhibitor) treatments significantly elevated ALP activity compared with the LPS-treated group alone ($P < 0.001$) (Figure 4D). Protein blot analysis (Figure 4E) showed that GB and BAY11-7082 treatments significantly up-regulated the expression levels of the osteogenesis-related proteins ALP (Figure 4F), RUNX-2 (Figure 4G), and COL-1 (Figure 4H) ($P < 0.001$). These findings suggested that the NF-κB pathway was inhibited, and the primitive osteogenesis was suppressed, establishing NF-κB pathway regulation as the central mechanism through which GB rescues osteogenic differentiation potential in inflammatory microenvironments.

Measurement of NF-κB Pathway Activation Time

To determine the optimal time point for NF-κB pathway activation after the addition of LPS, we chose to detect p-NF-κB protein expression at five time points, namely, 0, 5 min, 15 min, 60 min and 240 min. The experimental results suggested that the up-regulation of p-NF-κB protein expression could be detected after 5 min of adding LPS treatment, and then the expression continued to increase, and phosphorylation levels exhibited progressive elevation, peaking at 60 min before gradually returning to basal levels by 240 min (Figure 5A and B). Based on this time-effect relationship, the time node of adding LPS for 60 min was selected as the key detection time point of NF-κB pathway-related proteins in the subsequent experiments. The rapid and transient nature of this response suggests tight temporal regulation of inflammatory signaling in HPDLSCs, with the peak activation window representing the most biologically relevant period for therapeutic intervention.

GB Inhibits NF-κB Pathway Activation to Rescue Osteogenic Differentiation

Western blot analysis demonstrated that both GB and BAY11-7082 treatments significantly reduced LPS-induced phosphorylation of NF-κB and IκBα compared to LPS treatment alone (Figure 5C–E). The suppression of these phosphorylated proteins by GB was comparable to that achieved by the specific NF-κB inhibitor BAY11-7082. This

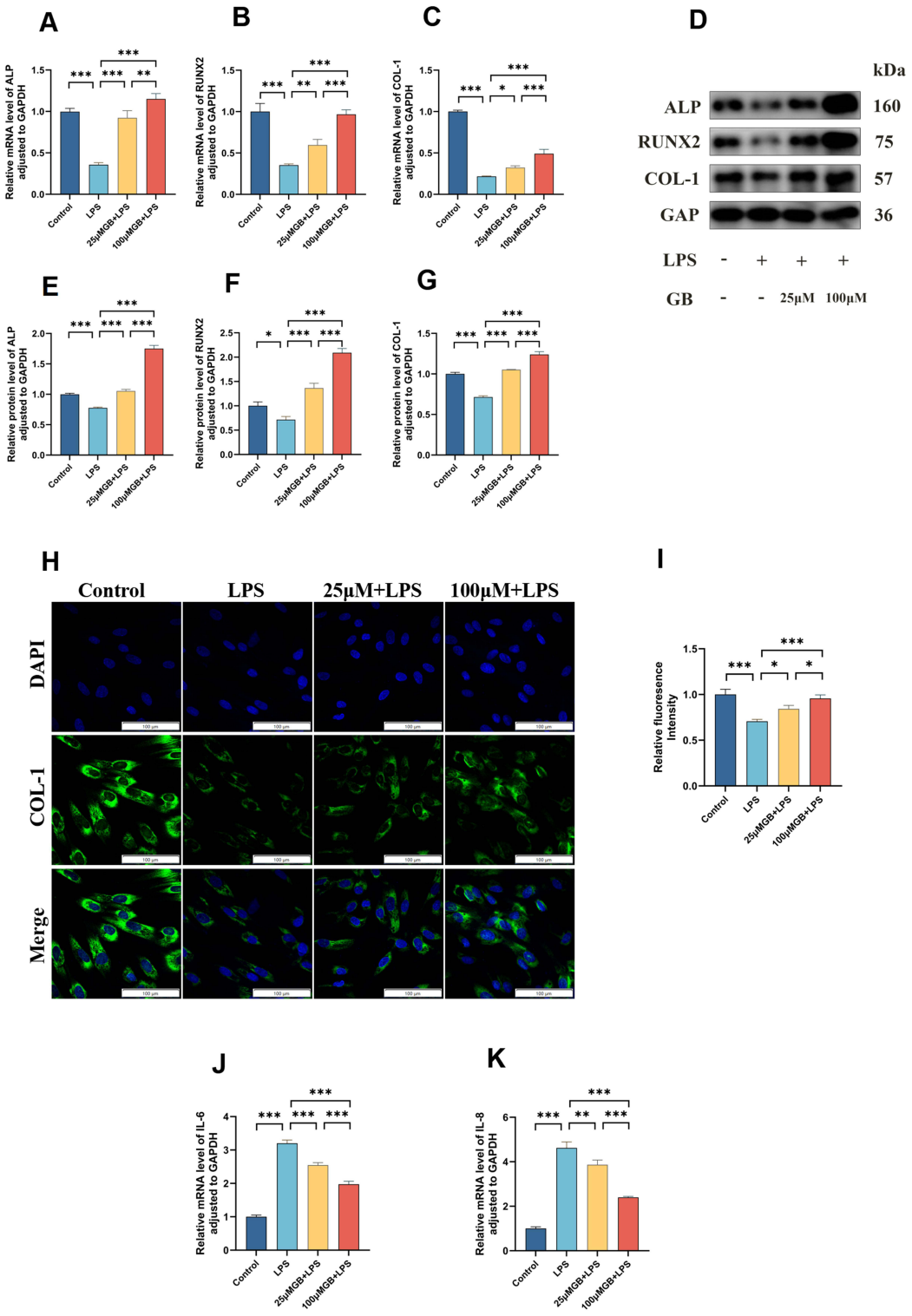

Figure 3 GB rescues LPS-induced inhibition of osteogenesis in HPDLSCs. (**A**–**C**) Semi-quantitative analysis of the protein expression level of ALP, RUNX-2 and COL-1 in HPDLSCs after osteogenic induction for 14 days under control, LPS (1 μg/mL) or LPS (1 μg/mL) and ginkgolide B (25 μM, 100 μM) treatment (one-way ANOVA). Error bars stand for mean ± SD. *P < 0.05, ***P < 0.001. (**D**) Western blot assay for ALP, RUNX-2 and COL-1 protein expression in HPDLSCs after osteogenic induction for 14 days under control, LPS (1 μg/mL) or LPS (1 μg/mL) and ginkgolide B (25 μM, 100 μM) treatment. (**E**–**G**) The mRNA expression level of ALP, RUNX-2 and COL-1 in HPDLSCs after osteogenic induction for 14 days under control, LPS (1 μg/mL) or LPS (1 μg/mL) and ginkgolide B (25 μM, 100 μM) treatment (one-way ANOVA). Error bars stand for mean ± SD. *P < 0.05, **P < 0.01, ***P < 0.001. (**H**) Immunofluorescence detection of the expression of COL-1. Scale bar: 100 μm. (**I**) Quantitative detection of COL-1 immunofluorescence intensity (one-way ANOVA). Error bars stand for mean ± SD. *P < 0.05, ***P < 0.001. (**J** and **K**) Relative IL-6 (**J**) and IL-8 (**K**) mRNA expression level in HPDLSCs after osteogenic induction for 14 days under control, LPS (1 μg/mL) or LPS (1 μg/mL) and ginkgolide B (25 μM, 100 μM) treatment (one-way ANOVA). Error bars stand for mean ± SD. **P < 0.01, ***P < 0.001. Each experiment was repeated five times.

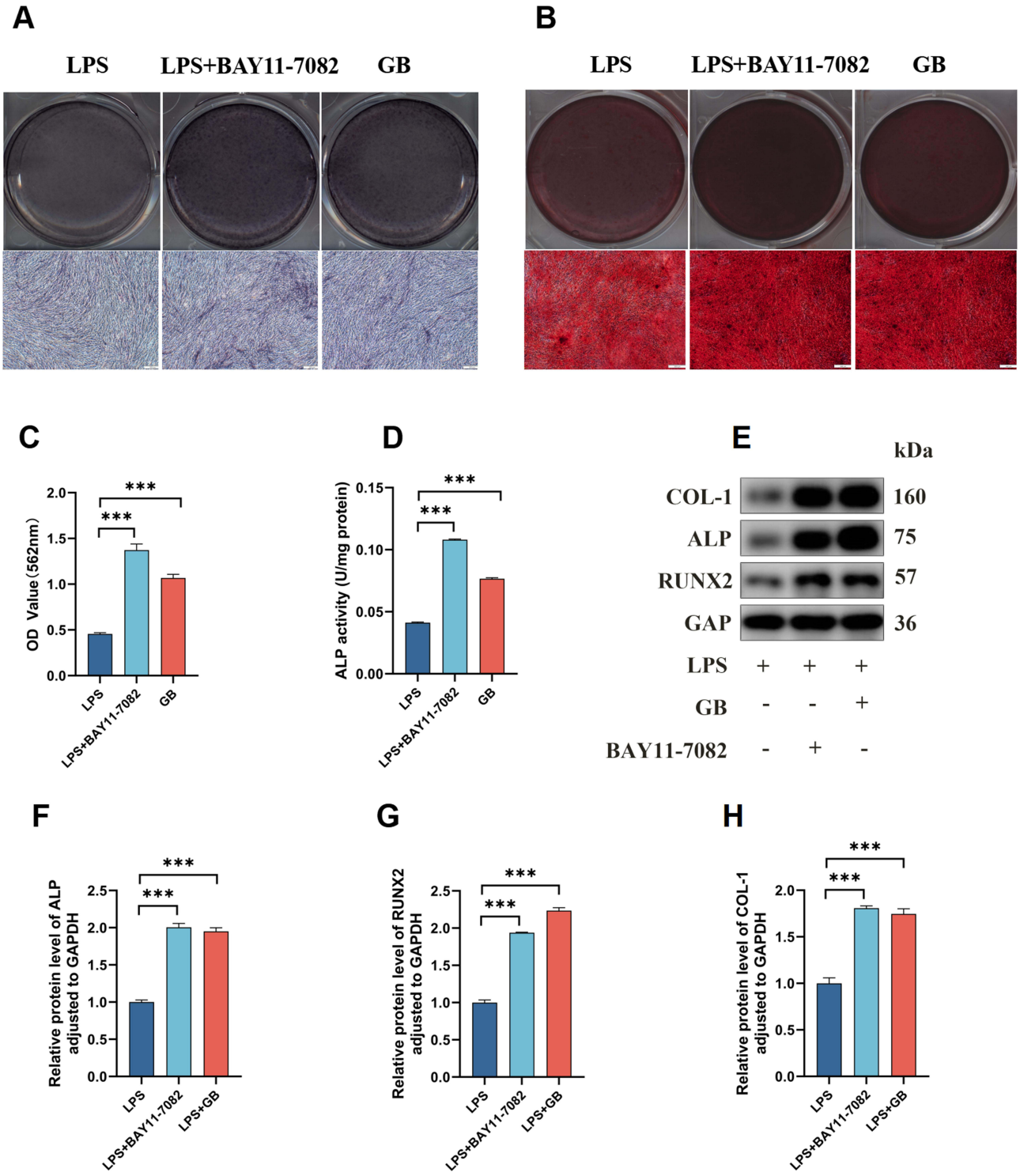

Figure 4 GB promoted osteogenic differentiation of HPDLSCs through the NF-κB pathway. (**A**) ALP staining under LPS (1 μg/mL), LPS (1 μg/mL) and BAY11-7082 or LPS (1 μg/mL) and ginkgolide B (100 μM) treatment for 7 days. Scale bar: 200 μm. (**B**) Formation of mineralized nodules under LPS (1 μg/mL), LPS (1 μg/mL) and BAY11-7082 or LPS (1 μg/mL) and ginkgolide B (100 μM) treatment for 28 days. Scale bar: 200 μm. (**C**) Extracellular matrix mineralisation was assessed at OD562 (one-way ANOVA). Error bars stand for mean ± SD. ***P < 0.001. (**D**) ALP activity under LPS (1 μg/mL), LPS (1 μg/mL) and BAY11-7082 or LPS (1 μg/mL) and ginkgolide B (100 μM) treatment for 7 days (one-way ANOVA). Error bars stand for mean ± SD. ***P < 0.001. (**E**) Western blot assay for ALP, RUNX-2 and COL-1 protein expression level in HPDLSCs after osteogenic induction for 14 days under LPS (1 μg/mL), LPS (1 μg/mL) and BAY11-7082 or LPS (1 μg/mL) and ginkgolide B (100 μM) treatment. (**F–H**) Semi-quantitative analysis of ALP, RUNX-2 and COL-1 in HPDLSCs after osteogenic induction for 14 days under LPS (1 μg/mL), LPS (1 μg/mL) and BAY11-7082 or LPS (1 μg/mL) and ginkgolide B (100 μM) treatment (one-way ANOVA). Error bars stand for mean ± SD. ***P < 0.001. Each experiment was repeated five times.

https://doi.org/10.2147/DDDT.S541290

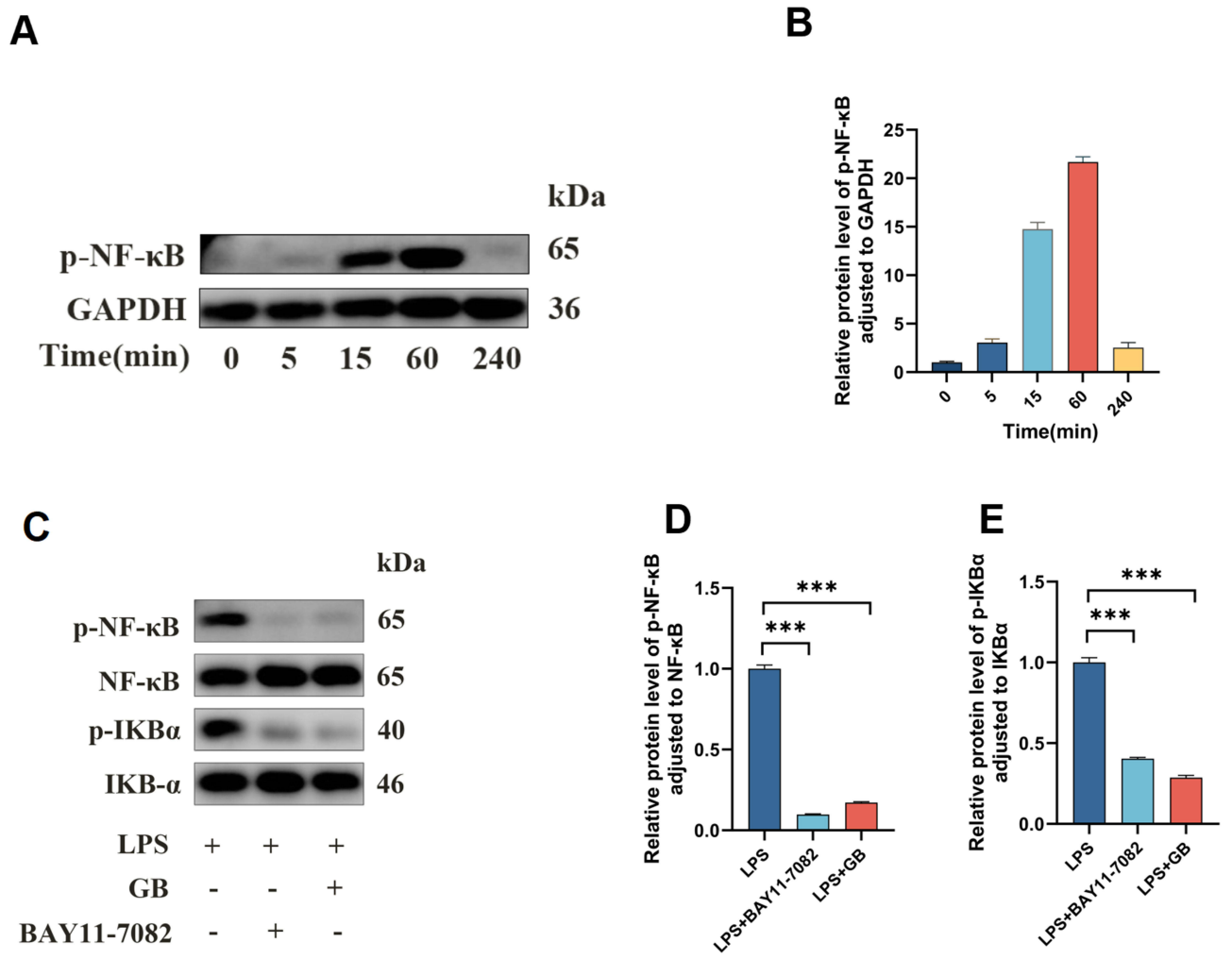

Figure 5 GB rescues LPS-induced inhibition of osteogenesis in HPDLSCs via the p-IκBα/NF-κB pathway. (**A** and **B**) Activation of the NF-κB pathway after the addition of LPS at different time points. (**A**) Western blot assay for p-NF-κB protein expression in HPDLSCs after osteogenic induction for 14 days under LPS (1 μg/mL) treatment. (**B**) Semi-quantitative analysis of p-NF-κB protein levels in HPDLSCs (one-way ANOVA). Error bars stand for mean ± SD. (**C**) The protein expression level of p-NF-κB, NF-κB, p-IκBα and IκBα in HPDLSCs after osteogenic induction for 14 days under LPS, LPS (1 μg/mL) and BAY11-7082, LPS (1 μg/mL) and ginkgolide B (100 μM) treatment. (**D** and **E**) Relative quantification of p-NF-κB/NF-κB (**D**) and p-IκBα/IκBα (**E**) protein expression level (one-way ANOVA). Error bars stand for mean ± SD. ***P < 0.001. Each experiment was repeated five times.

parallel suppression of both phosphorylation events confirms that GB effectively targets the NF-κB signaling cascade at multiple regulatory points, with efficacy comparable to a canonical pathway inhibitor.

Periodontitis Model Validation and Micro-CT Analysis

A rat periodontitis model was established (Figure 6A and B). During the experimental period, systemic health monitoring revealed no treatment-related abnormalities, supporting the safety profile of GB administration. (Figure 6C). Micro-CT results showed that, compared with the control group, there was significant resorption of the alveolar bone around the second molars in the MOD group, and the distance from the cemento-enamel junction to the alveolar bone crest was significantly increased, while GB treatment groups displayed dose-dependent attenuation of bone loss (Figure 6D and E) ($P < 0.01$, $P < 0.001$). BMD and BV/TV analyses showed the same trend: the BMD and BV/TV values were significantly lower in the MOD group than in the control group, and showed a dose-dependent rebound in the GB-treated group (Figure 6F and G) ($P < 0.01$, $P < 0.001$). These comprehensive findings demonstrate GB's capacity to preserve both structural integrity and bone quality in experimental periodontitis while maintaining excellent safety characteristics.

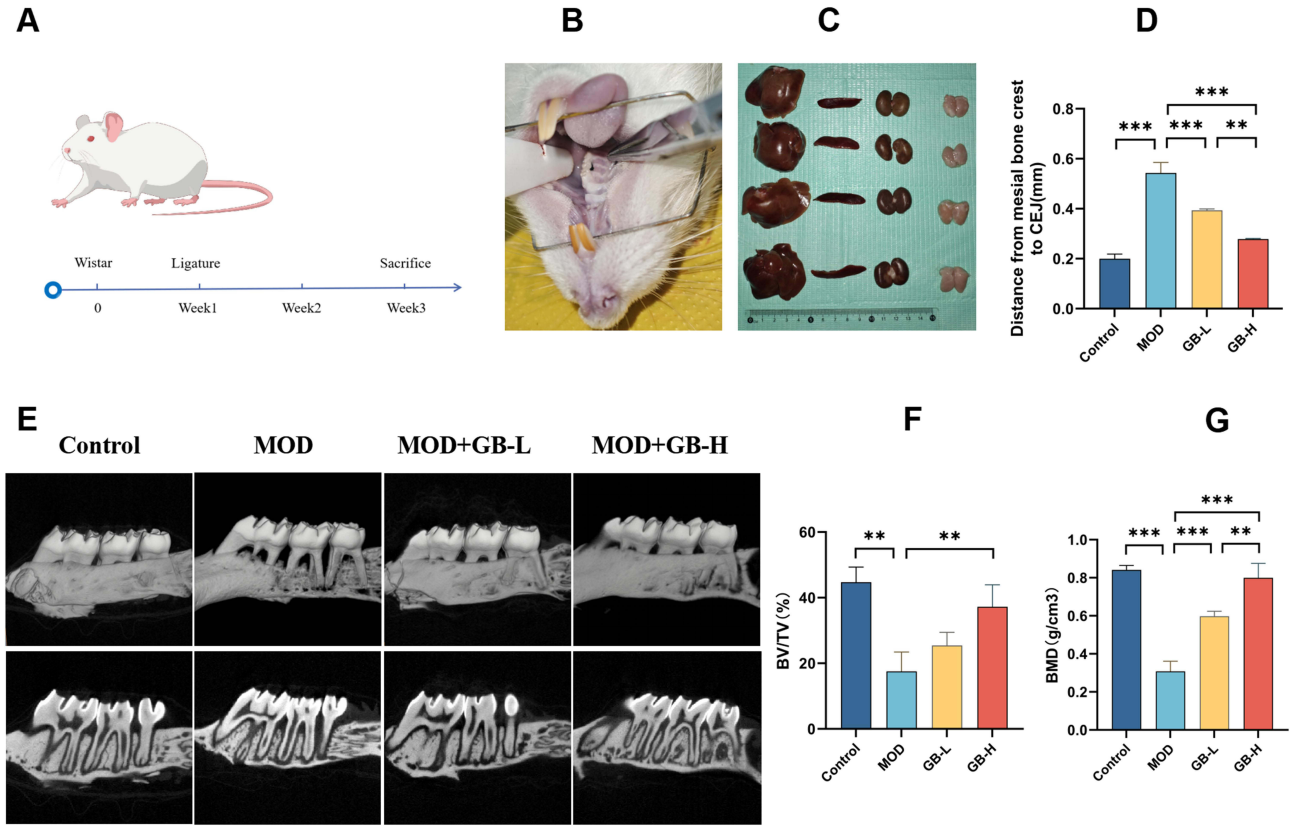

Figure 6 The establishment of the periodontitis model and three-dimensional reconstruction analysis of sample data. (**A**) The process of animal experiment (Created with BioGDP.com).[30] (**B**) Periodontitis model in rats. (**C**) Diagram of internal organs of rats in each group. (**E**) Representative micro-CT scanning images along the longitudinal direction of the maxilla and stereomicroscopic images. (**D**–**G**) Quantitative analysis of bone indices associated with rat alveolar bone, including CEJ-ABC (D), BV/TV (**F**) and BMD (G). CEJ: Cemento-enamel junction. ABC: Alveolar bone crest. BMD: Bone mineral density (one-way ANOVA). Error bars stand for mean ± SD (n=9). **P < 0.01, ***P < 0.001.

HE, MASSON and TRAP Staining Observation

Histomorphological analysis revealed distinct pathological changes across experimental groups. HE staining and MASSON staining (Figure 7A) showed that compared with the control group, the alveolar bone height in the second molar region of the MOD group was significantly reduced, with sparse and disorganized trabecular structure and abnormal collagen fiber arrangement; whereas the alveolar bone resorption in the low-dose group (MOD+GB-L) and high-dose group (MOD+GB-H) groups was reduced, with a more intact trabecular structure and a regular arrangement of collagen fibers. TRAP staining (Figure 7B) showed that positive multinucleated cells (osteoclasts) were distributed on the top surface of the alveolar ridge, with bone resorption traps around the cells. The number of osteoclasts at the top of the alveolar ridge in the proximal middle of the second molar (Figure 7C) increased in the MOD group compared with the control group ($P < 0.001$), and the number of osteoclasts rebounded in the GB-treated group ($P < 0.05$, $P < 0.001$). The preserved bone morphology and reduced number of osteoclasts in GB-treated animals correlate with the Micro-CT findings, demonstrating GB's multifaceted protection against periodontitis-induced bone destruction.

IHC Staining Analysis

IHC staining was performed to assess the immunoreactivity of RANKL and RUNX-2 in periodontal ligament (PDL). The expression level of RANKL and RUNX-2 was decreased in the MOD group compared to the control group ($P < 0.001$), and the expression of these molecules was increased in the GB-treated group compared to the MOD group (Figure 7D–F) ($P < 0.01$, $P < 0.001$). The differential restoration of RUNX-2 and RANKL suggests GB promotes anabolic processes, providing mechanistic insight into its alveolar bone-preserving effects observed in micro-CT and histological analyses.

https://doi.org/10.2147/DDDT.S541290

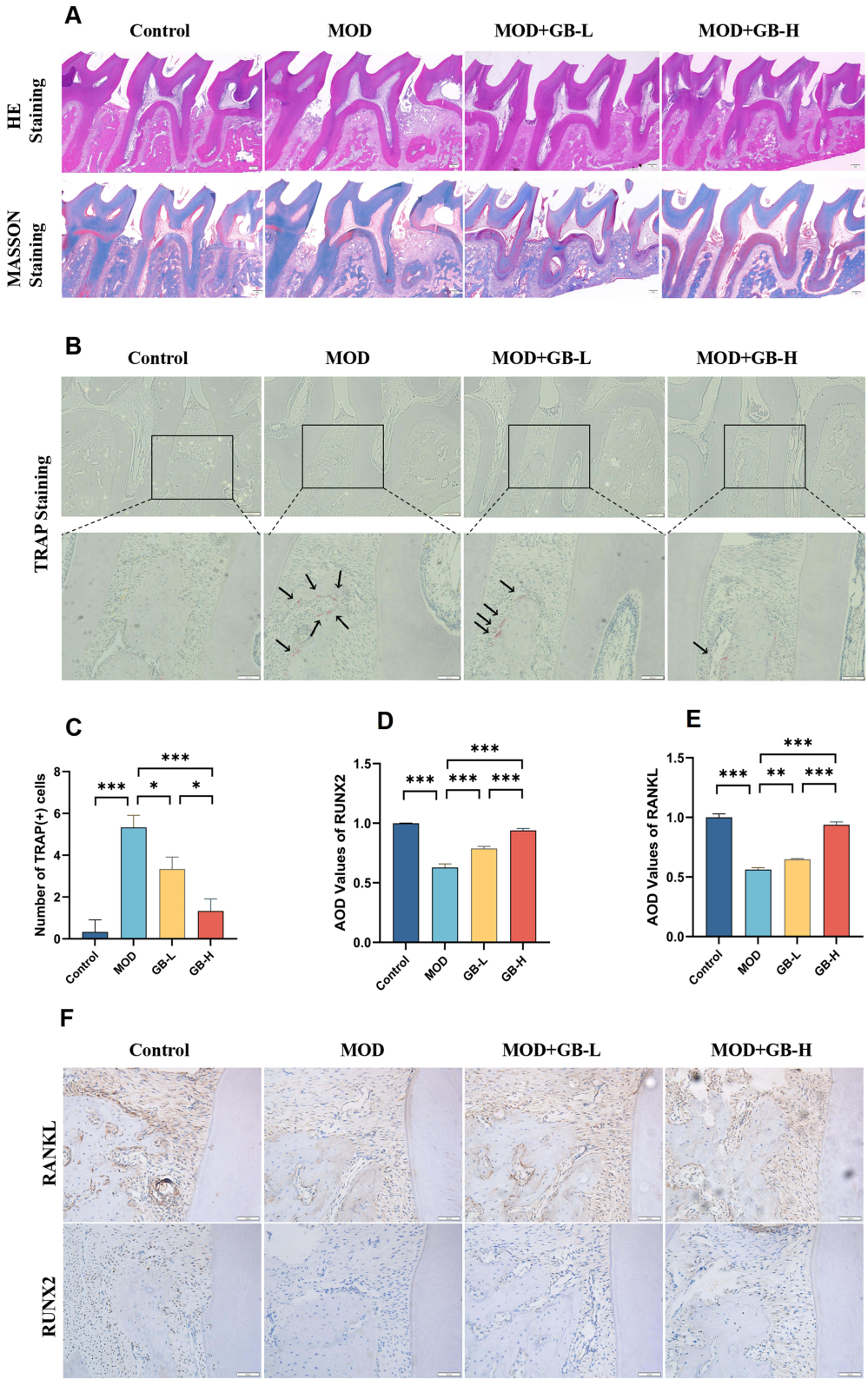

Figure 7 Results of HE, MASSON and TRAP staining. (**A**) HE staining of periodontal tissue. Scale bar: 200 μm. (**B**) Representative TRAP staining images of alveolar bone, highlighting TRAP-positive osteoclasts with black arrows. Scale bar: 200 μm or 50 μm. (**C**) The number of TRAP-positive cells (one-way ANOVA). Error bars stand for mean ± SD (n=9). *P < 0.05, ***P < 0.001. (**D**–**E**) The AOD values of RUNX-2 (**D**) and RANKL (**E**) (one-way ANOVA). Error bars stand for mean ± SD (n=9). **P < 0.01, ***P < 0.001. (**F**) The immunoreactivity of RUNX-2 and RANKL. Scale bar: 50 μm.

 https://doi.org/10.2147/DDDT.S541290

Discussion

Periodontitis, a widely prevalent inflammatory disease of the oral cavity worldwide, is the leading cause of tooth loss and poses a major challenge to oral health. Traditional chemotherapy faces limitations such as drug resistance and microbial imbalance, while herbal natural products are potential alternatives due to their high safety profile and multi-targeted effects.[31] In previous studies, GB, as a natural anti-inflammatory product, has demonstrated significant anti-inflammatory effects. Our study aimed to elucidate GB's role in counteracting inflammation-mediated osteogenic disruption and its mechanism, potentially offering new periodontitis treatment options.

As a major active constituent of Ginkgo biloba extract, GB exhibits diverse pharmacological properties, including anti-inflammatory, antioxidant, and autophagy-modulating effects, which have been extensively studied in neurological and cardiovascular disorders.[32–34] As a specific antagonist of platelet-activating factor (PAF),[35] GB demonstrates significant neuroprotective effects by suppressing NLRP3 inflammasome activation.[36] These mechanism contributes to its ability to alleviate neuropathic pain and mitigate cognitive dysfunction in neurodegenerative disorders such as Alzheimer's and Parkinson's diseases.[37–39] In cardiovascular diseases, it exerts anti-atherosclerotic and endothelial protective effects[40] through modulation of NADPH oxidase, LOX-1, and SIRT1 pathways.[41–43] Additionally, GB modulates key cellular processes including senescence, apoptosis, and oxidative stress.[44,45] In periodontal tissues, aging induces oxidative stress through ROS overproduction from mitochondrial dysfunction, DNA damage, and cytokine signaling. This redox imbalance triggers NF-κB activation, enhancing osteoclastogenesis while suppressing osteogenesis through increased osteoblast apoptosis.[46] Despite these well-documented systemic benefits, research on GB's role in oral diseases, particularly periodontitis, remains limited. Given its ability to dampen inflammatory cascades, counteract oxidative damage, and promote cellular homeostasis, GB holds significant promise as a therapeutic agent for periodontal therapy.

Chronic periodontitis is an inflammatory disease of the dental plaque. Porphyromonas gingivalis is one of the most widely studied causative agents of periodontitis and is often considered to be the main etiological factor in the progression of periodontitis, secreting several virulence factors (LPS) and extracellular proteases (Porphyromonas gingivalis proteases), which destroy the tissues surrounding the teeth.[47–50] In addition, LPS has been observed to inhibit osteogenesis by enhancing the release of pro-inflammatory factors through activation of the NF-κB pathway,[51] and blocking the NF-κB signaling pathway partially reversed the LPS-induced decrease in the osteogenic capacity of rat periodontal stem cells.[52,53] In this experiment, HPDLSCs were treated with 1 μg/mL LPS, which induced inflammation formation and showed osteogenesis inhibition, and the mechanism was further explored by Western blot experiments.

This study presents novel evidence that ginkgolide B (GB) effectively treats periodontitis by inhibiting the NF-κB signal pathway. In vitro experiments demonstrated that GB (25 and 100 μM) reversed LPS-induced osteogenic suppression in HPDLSCs, restoring mineralization and osteogenic marker expression (ALP/RUNX-2/COL-1). In vivo, GB (5mg/kg/d and 20 mg/kg/d) reduced alveolar bone loss in periodontitis rats while normalizing bone density. Mechanistic studies revealed that GB suppresses NF-κB activation comparably to the specific inhibitor BAY11-7082,[54,55] inhibiting IκBα phosphorylation and subsequent NF-κB nuclear translocation. These findings establish GB as a dual-action therapeutic agent that simultaneously combats inflammation and promotes bone regeneration. This work expands GB's therapeutic potential from its established neuro/cardiovascular applications to periodontal disease, offering a promising multi-target approach for periodontitis management. As a natural anti-inflammatory agent, GB has a promising future in periodontitis treatment as its low toxicity and natural source properties provide advantages for its clinical application. However, there are still some issues that deserve further exploration, such as dose optimization and clinical translation, etc. In local oral applications, the pharmacokinetic characteristics and potential off-target effects of GB require particular attention. As a lipophilic compound, GB's poor water solubility results in low oral bioavailability and limited tissue penetration depth when administered locally in periodontal applications. Notably, significant variations exist in the absorption kinetics of GB across different ginkgo preparations, with bioavailability being directly influenced by formulation composition and extraction processes.[56] Achieving effective therapeutic concentrations often necessitates higher dosage levels, which not only approach toxicity thresholds but also elevate clinical safety risks.[42] Through an in-depth study of its molecular mechanism and optimization of the delivery strategy, GB is expected to become a new choice for the comprehensive treatment of periodontitis.

Conclusion

In summary, our study demonstrates that GB exerts dual therapeutic effects in periodontitis through NF-κB pathway inhibition. The experimental evidence reveals that GB (25–100 μM) not only suppresses LPS-induced inflammation in HPDLSCs but also rescues their osteogenic differentiation capacity, while in vivo administration significantly attenuates alveolar bone loss. These findings provide a solid experimental basis for GB as a naturally targeted drug for the treatment of periodontitis, and its property of exerting both anti-inflammatory and pro-regenerative effects through modulating the NF-κB pathway demonstrates significant clinical translational potential.

Abbreviations

GB, ginkgolide B; HPDLSCs, human periodontal ligament stem cells; LPS, lipopolysaccharide; CCK-8, Cell counting Kit-8; ARS, Alizarin Red Staining; ALP, alkaline phosphatase; RUNX-2, runx family transcription factor 2; COL-1, collagen type 1; qRT-PCR, quantitative reverse transcription polymerase chain reaction; NF-κB, nuclear factor kappa-B; micro-CT, Micro-computed tomography; IHC, immunohistochemical; ANOVA, analysis of variance; MSCs, mesenchymal stromal cells; α-MEM, α-minimum essential medium; PBS, phosphate-buffered saline; FBS, fetal bovine serum; OD, optical density; CPC, cetylpyridinium chloride; BCA, bicinchoninic acid; GAPDH, glyceraldehyde-3-phosphate dehydrogenase; AOD, average optical density; TBST, Tris-buffered saline containing 0.1% Tween 20; BSA, bovine serum albumin; DAPI, 4,6-diamidino-2-phenylindole; SPF, specific pathogen-free; ROI, region of interest; BMD, bone mineral density; BV/TV, bone volume/total volume; CEJ, cemento-enamel junction; ABC, alveolar bone crest; PDL, periodontal ligament; HE, hematoxylin and eosin; TRAP, tartaric-resistant acid phosphatase; RANKL, nuclear factor-κB (NF-κB) ligand.

Acknowledgments

This work was supported by the Province Natural Science Foundation of Shandong Province, grant number ZR2021QH340.

Disclosure

The authors report no conflicts of interest in this work.

References

1. Nascimento GG, Alves-Costa S, Romandini M. Burden of severe periodontitis and edentulism in 2021, with projections up to 2050: the global burden of disease 2021 study. *J Periodontal Res*. 2024;59(5):823–867. doi:10.1111/jre.13337
2. Uy SNMR, Deng K, Fok CTC, Fok MR, Pelekos G, Tonetti MS. Food intake, masticatory function, tooth mobility, loss of posterior support, and diminished quality of life are associated with more advanced periodontitis stage diagnosis. *J Clin Periodontol*. 2022;49(3):240–250. doi:10.1111/jcpe.13588
3. Logan D, McEvoy CT, McKenna G, Kee F, Linden G, Woodside JV. Association between oral health status and future dietary intake and diet quality in older men: the PRIME study. *J Dent*. 2020;92:103265. doi:10.1016/j.jdent.2019.103265
4. Nisanci Yilmaz MN, Bulut S, Bakirarar B. Impact of stage-grade of periodontitis and self-reported symptoms on oral health-related quality of life. *Int J Dent Hyg*. 2022;20(2):291–300. doi:10.1111/idh.12551
5. Agnese CCD, Schöffer C, Kantorski KZ, Zanatta FB, Susin C, Antoniazzi RP. Periodontitis and oral health–related quality of life: a systematic review and meta-analysis. *J Clin Periodontol*. 2025;52(3):408–420. doi:10.1111/jcpe.14074
6. Han S, Ko Y, Ham LK, Park JH, Kim Y. Precautions and possibilities in orthodontic treatment of periodontally compromised patients: current recommendations. *J Esthet Restor Dent*. 2024;36(4):595–605. doi:10.1111/jerd.13166
7. Polizzi A, Alibrandi A, Lo Giudice A, et al. Impact of periodontal microRNAs associated with alveolar bone remodeling during orthodontic tooth movement: a randomized clinical trial. *J Transl Med*. 2024;22(1):1155. doi:10.1186/s12967-024-05933-x
8. Ryoo KS, Kim KH, Cho YD, Seol YJ, Ku Y. Effects of adjacent periodontitis on osseointegrated dental implants. *J Periodontal Implant Sci*. 2024;54(4):280. doi:10.5051/jpis.2302400120
9. Isola G, Polizzi A, Santagati M, Alibrandi A, Iorio-Siciliano V, Ramaglia L. Effect of nonsurgical mechanical debridement with or without chlorhexidine formulations in the treatment of peri-implant mucositis. a randomized placebo-controlled clinical trial. *Clin Oral Implants Res*. 2025;36(5):566–577. doi:10.1111/clr.14405
10. Chiang N, Serhan CN. Specialized pro-resolving mediator network: an update on production and actions. *Essays Biochem*. 2020;64(3):443–462. doi:10.1042/EBC20200018
11. Rapone B, Inchingolo F, Tartaglia GM, De Francesco M, Ferrara E. Asymmetric dimethylarginine as a potential mediator in the association between periodontitis and cardiovascular disease: a systematic review of current evidence. *Dent J*. 2024;12(9):297. doi:10.3390/dj12090297
12. Lu L, Zhao D, Li C, et al. The role of periodontitis in the development of atherosclerotic cardiovascular disease in participants with the components of metabolic syndrome: a systematic review and meta-analysis. *Clin Oral Investig*. 2024;28(6):339. doi:10.1007/s00784-024-05731-1
13. Li Z, Li J, Huang X. Clinical trial landscape for periodontitis treatment: trend analysis and future perspectives. *J Transl Med*. 2024;22(1):907. doi:10.1186/s12967-024-05697-4

14. Sai Priya T, Ramalingam V, Suresh Babu K. Natural products: a potential immunomodulators against inflammatory-related diseases. *Inflammopharmacology*. 2024;32(5):2821–2859. doi:10.1007/s10787-024-01562-4
15. Upton JEM, Grunebaum E, Sussman G, Vadas P. Platelet activating factor (PAF): a mediator of inflammation. *BioFactors*. 2022;48(6):1189–1202. doi:10.1002/biof.1883
16. Jiang Q, Lu M, Li J, Zhu Z. Ginkgolide B protects cardiomyocytes from angiotensin ii-induced hypertrophy via regulation of autophagy through SIRT1-FoxO1. *Cardiovasc Ther*. 2021;2021:1–9.
17. Wang BY, Chen Y, Hsiao AW, Chen W, Lee C, Lee OK. Ginkgolide B facilitates muscle regeneration via rejuvenating osteocalcin-mediated bone-to-muscle modulation in aged mice. *J Cachexia, Sarcopenia Muscle*. 2023;14(3):1349–1364. doi:10.1002/jcsm.13228
18. Mazziotta C, Badiale G, Cervellera CF, Tognon M, Martini F, Rotondo JC. Regulatory mechanisms of circular RNAs during human mesenchymal stem cell osteogenic differentiation. *Theranostics*. 2024;14(1):143–158. doi:10.7150/thno.89066
19. Du A, Zhao S, Wan L, et al. Micro RNA expression profile of human periodontal ligament cells under the influence of Porphyromonas gingivalis LPS. *J Cell Mol Med*. 2016;20(7):1329–1338. doi:10.1111/jcmm.12819
20. Chen H, Zhang L, Du S, et al. Triptolide mitigates the inhibition of osteogenesis induced by TNF-α in human periodontal ligament stem cells via the p-IκBα/NF-κB signaling pathway: an in-vitro study. *BMC Complement Med Ther*. 2024;24(1):113. doi:10.1186/s12906-024-04408-2
21. Chu C, Ru H, Chen Y, Xu J, Wang C, Jin Y. Gallic acid attenuates LPS-induced inflammation in Caco-2 cells by suppressing the activation of the NF-κB/MAPK signaling pathway. *Acta Biochim Biophys Sin*. 2024;56(6):905–915. doi:10.3724/abbs.2024008
22. Chen CY, Kao CL, Liu CM. The cancer prevention, anti-inflammatory and anti-oxidation of bioactive phytochemicals targeting the TLR4 signaling pathway. *Int J Mol Sci*. 2018;19(9):2729. doi:10.3390/ijms19092729
23. Xu H, Wang T, Yang Y. BPIFA1 inhibits periodontitis by regulating the NF-κB/IκB signaling pathway and macrophage M1/M2 polarization. *Arch Oral Biol*. 2025;173:106190. doi:10.1016/j.archoralbio.2025.106190
24. Yao X, Liu M, Wang P. Sitagliptin regulates the AMPK/NF-κB signaling pathway to alleviate lipopolysaccharide-induced inflammatory responses and promote osteogenic differentiation in rat bone marrow mesenchymal stem cells. *Arch Oral Biol*. 2025;175:106253. doi:10.1016/j.archoralbio.2025.106253
25. Zhang R, Xu L, Zhang D, et al. Cardioprotection of ginkgolide b on myocardial ischemia/reperfusion-induced inflammatory injury via regulation of A20-NF-κB pathway. *Front Immunol*. 2018;9:2844. doi:10.3389/fimmu.2018.02844
26. Xiang Y, Zhang S, Lu J, et al. Ginkgolide B protects human pulmonary alveolar epithelial A549 cells from lipopolysaccharide-induced inflammatory responses by reducing TRIM37-mediated NF-κB activation. *Biotechnol Appl Biochem*. 2020;67(6):903–911. doi:10.1002/bab.1847
27. Lee CW, Lin HC, Wang BYH, et al. Ginkgolide B monotherapy reverses osteoporosis by regulating oxidative stress-mediated bone homeostasis. *Free Radic Biol Med*. 2021;168:234–246. doi:10.1016/j.freeradbiomed.2021.03.008
28. Zhu B, Xue F, Zhang C, Li G. Ginkgolide B promotes osteoblast differentiation via activation of canonical Wnt signalling and alleviates osteoporosis through a bone anabolic way. *J Cell Mol Med*. 2019;23(8):5782–5793. doi:10.1111/jcmm.14503
29. Huang J, Yang J, Zou X, et al. Ginkgolide B promotes oligodendrocyte precursor cell differentiation and survival via Akt/CREB/bcl-2 signaling pathway after white matter lesion. *Exp Biol Med*. 2021;246(10):1198–1209. doi:10.1177/1535370221989955
30. Jiang S, Li H, Zhang L, et al. Generic Diagramming Platform (GDP): a comprehensive database of high-quality biomedical graphics. *Nucleic Acids Res*. 2025;53(D1):D1670–D1676. doi:10.1093/nar/gkae973
31. Xing A, Wang F, Liu J, et al. The prospect and underlying mechanisms of Chinese medicine in treating periodontitis. *Chin J Nat Med*. 2025;23(3):269–285. doi:10.1016/S1875-5364(25)60842-9
32. Li J, Jia S, Song Y, Xu W, Lin J. Ginkgolide B can alleviate spinal cord glymphatic system dysfunction and provide neuroprotection in painful diabetic neuropathy rats by inhibiting matrix metalloproteinase-9. *Neuropharmacology*. 2024;250:109907. doi:10.1016/j.neuropharm.2024.109907
33. Yang T, Du X, Xu L. Radioprotective effect of Ginkgolide B on brain: the mediating role of DCC/MST1 signaling. *Int J Radiat Biol*. 2024;100(3):371–384. doi:10.1080/09553002.2023.2281515
34. Zhang Y, Zhao Y, Zhang J, et al. Quantitative proteomics reveals neuroprotective mechanism of ginkgolide B in Aβ1-42-induced N2a neuroblastoma cells. *J Integr Neurosci*. 2023;22(2):33. doi:10.31083/j.jin2202033
35. Shang Q, Zhou X, Yang MR, et al. Amide derivatives of ginkgolide B and their inhibitory effects on PAF-induced platelet aggregation. *ACS Omega*. 2021;6(35):22497–22503. doi:10.1021/acsomega.1c01682
36. Liang JH, Yu H, Xia CP, et al. Ginkgolide B effectively mitigates neuropathic pain by suppressing the activation of the NLRP3 inflammasome through the induction of mitophagy in rats. *Biomed Pharmacother*. 2024;177:117006. doi:10.1016/j.biopha.2024.117006
37. Luo T, Hao YN, Lin DD, Huang X, Wu AS. Ginkgolide B improved postoperative cognitive dysfunction by inhibiting microgliosis-mediated neuroinflammation in the hippocampus of mice. *BMC Anesthesiol*. 2022;22(1):229. doi:10.1186/s12871-022-01750-1
38. Gachowska M, Szlasa W, Saczko J, Kulbacka J. Neuroregulatory role of ginkgolides. *Mol Biol Rep*. 2021;48(7):5689–5697. doi:10.1007/s11033-021-06535-2
39. Wang Q, Ma R, Liu P, et al. Efficient sustained-release nanoparticle delivery system protects nigral neurons in a toxin model of Parkinson's disease. *Pharmaceutics*. 2022;14(8):1731. doi:10.3390/pharmaceutics14081731
40. Pius Bassey A, Zhang Y, Wu H, et al. Untargeted metabolomics unravels the effects of ginkgolide B-producing Lactiplantibacillus plantarum and co-induced fermentation of ginkgo kernel juice and their underlying vascular endothelial cell protection activity. *Food Res Int*. 2024;197:115168. doi:10.1016/j.foodres.2024.115168
41. Liu Y, Zhang C, Cheng L, Wang H, Lu M, Xu H. Enhancing both oral bioavailability and anti-ischemic stroke efficacy of ginkgolide B by preparing nanocrystals self-stabilized Pickering nano-emulsion. *Eur J Pharm Sci*. 2024;192:106620. doi:10.1016/j.ejps.2023.106620
42. Ye W, Wang J, Little PJ, et al. Anti-atherosclerotic effects and molecular targets of ginkgolide B from Ginkgo biloba. *Acta Pharm Sin B*. 2024;14(1):1–19. doi:10.1016/j.apsb.2023.09.014
43. Wu T, Li D, Chen Q, et al. Identification of VDAC1 as a cardioprotective target of Ginkgolide B. *Chem Biol Interact*. 2025;406:111358. doi:10.1016/j.cbi.2024.111358
44. Ding X, Tan D, Wang Z, Yin H. Ginkgolide B regulates apoptosis, oxidative stress, and mitochondrial dysfunction in MPP+-induced SK-N-SH cells by targeting HDAC4/JNK pathway. *Naunyn Schmiedebergs Arch Pharmacol*. 2025;398(7):8899–8908. doi:10.1007/s00210-025-03815-7
45. Xu H, Zhou Z, Wen F, Sun H, Hou J. Inhibiting autophagy further promotes Ginkgolide B's anti-osteoclastogenesis ability. *Bone*. 2025;192:117348. doi:10.1016/j.bone.2024.117348

46. Yu B, Wang C. Osteoporosis and periodontal diseases – an update on their association and mechanistic links. *Periodontol 2000*. 2022;89(1):99–113. doi:10.1111/prd.12422
47. Gasmi A, Gasmi BA, Noor S, Mujawdiya P. Porphyromonas Gingivalis in the Development of periodontitis: impact on dysbiosis and inflammation. *Arch Razi Inst*. 2022;77(5):1539–1551. doi:10.22092/ARI.2021.356596.1875
48. Rafiei M, Kiani F, Sayehmiri F, Sayehmiri K, Sheikhi A, Zamanian Azodi M. Study of Porphyromonas gingivalis in periodontal diseases: a systematic review and meta-analysis. *Med J Islam Repub Iran*. 2017;31(1):355–362. doi:10.14196/mjiri.31.62
49. Li R, Huang Z, Chen M. Long non-coding RNA EPB41L4A-AS1 serves as a diagnostic marker for chronic periodontitis and regulates periodontal ligament injury and osteogenic differentiation by targeting miR-214-3p/YAP1. *J Inflamm Res*. 2025;18:2483–2497. doi:10.2147/JIR.S491724
50. Nativel B, Couret D, Giraud P, et al. Porphyromonas gingivalis lipopolysaccharides act exclusively through TLR4 with a resilience between mouse and human. *Sci Rep*. 2017;7(1):15789. doi:10.1038/s41598-017-16190-y
51. Sandra F, Sudiono J, Chouw A, Celinna M, Dewi NM, Djamil MS. Inhibition of lipopolysaccharide-induced NF-κB maintains osteogenesis of dental pulp and periodontal ligament stem cells. *Braz Oral Res*. 2024;38:e037.
52. Li C, Li B, Dong Z, et al. Lipopolysaccharide differentially affects the osteogenic differentiation of periodontal ligament stem cells and bone marrow mesenchymal stem cells through Toll-like receptor 4 mediated nuclear factor κB pathway. *Stem Cell Res Ther*. 2014;5(3):67. doi:10.1186/scrt456
53. Chen M, Lin X, Zhang L, Hu X. Effects of nuclear factor-κB signaling pathway on periodontal ligament stem cells under lipopolysaccharide-induced inflammation. *Bioengineered*. 2022;13(3):7951–7961. doi:10.1080/21655979.2022.2051690
54. Moon J, Moon IJ, Hyun H, et al. Bay 11-7082, an NF - κB inhibitor, prevents post-inflammatory hyperpigmentation through inhibition of inflammation and melanogenesis. *Pigm Cell Melanoma Res*. 2025;38(1):e13207. doi:10.1111/pcmr.13207
55. Guruvaiah P, Gupta R. IκBα kinase inhibitor BAY 11-7082 promotes anti-tumor effect in RAS-driven cancers. *J Transl Med*. 2024;22(1):642. doi:10.1186/s12967-024-05384-4
56. Woelkart K, Feizlmayr E, Dittrich P, et al. Pharmacokinetics of bilobalide, ginkgolide A and B after administration of three different Ginkgo biloba L. preparations in humans. *Phytother Res*. 2010;24(3):445–450. doi:10.1002/ptr.3074